Polarization-Dimension Competition in Centrosymmetric Flexoelectronic Transistors

Gongwei Hu[1], Yihan Zhang[1], Xiaoyu Lu[1], Yanshan Xiao[1, *], Junjun Hu[2,3,4], Chao Yong[2,3,4], Lijie Li[5, *], Wei Huang[2, *], and Fobao Huang[2,3, 4, *]

1. *Hubei Engineering Research Center of Weak Magnetic-field Detection, College of Science, China Three Gorges University, Yichang, 443002, China*

2. *State Key Laboratory of Flexible Electronics (LoFE) & School of Integrated Circuits (School of Microelectronics), Northwestern Polytechnical University, Xi'an 710072, China*

3. *Shenzhen Research Insititute of Northwestern Polytechnical University, Shenzhen 518057, China*

4. *Yangtze River Delta Research Institute of Northwestern Polytechnical University, Taicang 215400, China*

5. *Faculty of Science and Engineering, Swansea University, Swansea SA1 8EN, UK*

* Corresponding author email: yanshanxiao@foxmail.com; L.Li@swansea.ac.uk; iamwhuang@nwpu.edu.cn; fbhuang@nwpu.edu.cn

Abstract: Flexoelectricity that polarizes crystal by strain gradient offers an emerging interface engineering for the development of all-material functional electronics. As a new device paradigm, flexoelectronics enables the enhancement of electromechanical coupling in centrosymmetric semiconductors, however, the underline modulation is still required further understood. Here, we present a theoretical study of charge transport in silicon-based flexoelectronic transistors subjected to nanoscale tip loading. The results suggest that the mechanical load governs the current through two coupled mechanisms: strain-gradient-induced flexoelectric polarization that tunes the interfacial barrier, and load-dependent contact enlargement that introduces an additional, often non-negligible, dimensional contribution to conduction. These two effects act in opposite roles for p- and n-type devices, which causes a unique polarization–dimension competition for transport modulation. Moreover, increasing the tip radius weakens the polarization-driven modulation while strengthening the dimensional effect, providing a straightforward strategy to boost strain sensitivity via geometry design. These findings identify a distinctive regulation paradigm in flexoelectronic transistors and provide practical guidance for device optimization through geometry engineering.

Keywords: Flexoelectronic Transistor, Polarization–Dimension Competition, Interface Barrier, Centrosymmetric Semiconductors.

1. Introduction

With the rapid development of robot technology, artificial intelligence, and Internet of Things, polarization engineering using piezoelectric [1-4], pyroelectric [5,6], ferroelectric [7,8], and flexoelectric effects [9-13] has become increasingly crucial for new-emerging functional electronics. Among those effects, flexoelectricity, that uses a strain gradient to break inversion symmetry and thus induce an electrical polarization, is fundamentally universal in any solid [14,15]. This ubiquitous feature offers a symmetry-independent handle for manipulating physical responses and enabling multifunctional device concepts. Typical applications include triboelectricity [16,17], heterojunctions electronics [18], and tunneling [10,19], as well as bioelectronics [20,21], photoelectric detection [9,22], photovoltaic effect [23], pyroelectric effect [5], and transistors [11,12].

As an intrinsic electromechanical effect, flexoelectricity has also been used for mechanical sensing and mechanically reconfigurable electronics[10-12,19,24]. Pronounced electromechanical responses are reported by flexoelectric effect in both dielectrics [10,19] and nominally centrosymmetric materials [11,12]. For example, strain-gradient-induced polarization can activate conduction and yield large resistance modulation under mechanical loading [10]. Additionally, the generated polarization and its associated electrostatic potential can modulate Schottky barriers, greatly improving Si-based sensing performance [11]. Among these cases, a nanoscale tip is employed to generate ultralarge strain gradients, and thereby induce appreciable polarization even in weakly flexoelectric materials [25], such as Si, $SrTiO_3$ and TiO_2. Since this approach resembles piezotronics that uses strain-induced piezoelectric polarization charges for interface-barrier modulation [1-3,26], piezotronic effect are therefore often adopted to interpret various flexoelectronic transistor behaviors [11,12]. However, both effects are fundamentally different because piezotronics mainly relies on interface-localized polarization charges, whereas flexoelectricity produces bulk-distributed polarization charges. The latter complicates the modulation of interface barrier [10,19], leading to diverse transport properties and device functionality. Moreover, flexoelectric responses exhibit strong size and geometry dependence [27], especially under nanoindentation, where small variations in tip radius or contact conditions can markedly change the strain gradient and thus the polarization

strength and device output. Such sensitive size effect challenges device reproducibility and performance optimization. Therefore, a comprehensive understanding of flexoelectronic effect and its size effect in practical device configurations is highly required but still lacking.

In this work, we theoretically investigate the charge-transport characteristics of silicon-based flexoelectronic transistors under nanoscale tip loading. The results show that the applied load not only generates a strain-gradient-induced flexoelectric polarization that modulates the interfacial barrier, but also changes the contact size, which provides an additional and often non-negligible contribution to the transport current. Notably, the polarization-induced barrier tuning and the contact-dimension effect play opposite roles in regulating the output current for p-type and n-type devices, leading to a clear competition mechanism. Furthermore, increasing the tip radius suppresses the polarization contribution while amplifying the dimensional contribution, thereby offering an effective route to enhance the sensing performance. This study establishes a unified framework for interpreting flexoelectronic transistor responses and offer practical guidelines for performance optimization.

2. Carrier Transport in Centrosymmetric Flexoelectronic Transistors

When subjected to a tip force on material surface, the semiconductor such as centrosymmetric Si and TiO_2 endures a highly non-uniform strain over volume. Flexoelectric polarization are then induced to redistribute the carriers in a flexoelectronic transistor, where the tip acts also as a metal-semiconductor (MS) Schottky electrode. The present flexoelectronic transistor is fundamentally different from a conventional three-terminal field-effect transistor. In this device, the nanoscale tip plays two coupled roles simultaneously, i.e., the metal electrode that forms the Schottky contact with the semiconductor, and the mechanical loading that generates the strain gradient and induces flexoelectric polarization beneath the contact. Therefore, without tip contact, neither the metal–semiconductor interface nor the flexoelectric modulation exists, and the device is not established. The transport regulation discussed here thus originates from mechanically formed and mechanically modulated interface barriers, rather than from gate-voltage-controlled channel formation.

In MS Schottky junction, the carrier transport can be described from the physical equations of semiconductor devices, including the current density, current continuity, and electrostatic

equations [28]. The density equation demonstrates the current originated from carrier drift and diffusion mechanism can be expressed as

$$\boldsymbol{J}_n = q\mu_n n\boldsymbol{E} + qD_n\nabla n, \quad \boldsymbol{J}_p = q\mu_p p\boldsymbol{E} + qD_p\nabla p, \quad \boldsymbol{J}_T = \boldsymbol{J}_n + \boldsymbol{J}_p \tag{1}$$

where $\boldsymbol{J}_n$, $\boldsymbol{J}_p$ and $\boldsymbol{J}_T$ are the electron, hole and their total current, respectively. q is the element charge, n and p are the electron and hole concentration, $\boldsymbol{E}$ is the electrical field vector, μ_n and μ_p are the electron and hole mobility, and D_n and D_p are the electron and hole diffusion coefficient, $\boldsymbol{\nabla}$ is the gradient operation.

Another current-relevant equation is the charge continuity (charge conservation) given by

$$\frac{1}{q}\boldsymbol{\nabla}\cdot\boldsymbol{J}_n = U_n - G_n, \qquad \frac{1}{q}\boldsymbol{\nabla}\cdot\boldsymbol{J}_p = U_p - G_p \tag{2}$$

Here, U_n and U_p are the electron and hole recombination rate, and G_n and G_p are their generation rate.

In centrosymmetric semiconductor, strain gradient induces flexoelectric polarization to redistribute free carriers by adjusting potential at the MS interface. Such process can be described by adding an flexoelectric polarization in the Poisson equation [29,30]

$$\nabla\cdot\left[-\varepsilon_r\varepsilon_0\nabla V(\mathbf{r})\right] = q\left[N_D - N_A + p(x) - n(x)\right] - \nabla\cdot\mathbf{P}(\mathbf{r}) \tag{3}$$

where ε_r and ε_0 are the relative and vacuum permittivity, $\mathbf{P}(\boldsymbol{r})$ is the electric polarization induced here by flexoelectricity, N_D and N_A are the donor and acceptor doping concentration. The last term is flexoelectric charges $\rho_{flexo} = -\nabla\cdot\mathbf{P}(\mathbf{r})$ [11,12].

For an isotropous material, flexoelectric polarization is induced by flexoelectric effect under gradient strain [14]

$$P_i = \mu_{ijkl}\frac{\partial\varepsilon_{kl}}{\partial x_j} \tag{4}$$

Here, μ_{ijkl} is the flexoelectric coefficients, and $\partial\varepsilon_{kl}/\partial x_j$ stands for the gradient of strain component ε_{kl} in x_j direction, and Eq. (4) has used the Einstein summation. The flexoelectricity is a universal effect, and thereby presents in any materials.

Due to weak flexoelectric effect in centrosymmetric semiconductors, large strain gradient is required to produce evident flexoelectric polarization. A nanoscale tip is usually used and strain distribution can be described by a spherical indenter model [31]. The cylindrical

symmetry simplifies 3D indentation model into a 2D one. According to Eq. (4) (detailed see Note S1), the flexoelectric polarization is obtained as

$$\begin{pmatrix} P_r \\ P_z \end{pmatrix} = \begin{pmatrix} \varepsilon_{rr,r} & \varepsilon_{\theta\theta,r} + \varepsilon_{zz,r} & 2\varepsilon_{rz,z} \\ \varepsilon_{zz,z} & \varepsilon_{\theta\theta,z} + \varepsilon_{rr,z} & 2\varepsilon_{rz,r} \end{pmatrix} \begin{pmatrix} \mu_{11} \\ \mu_{14} \\ \mu_{111} \end{pmatrix} \tag{5}$$

Here, the strain gradient is $\varepsilon_{ij,k} = \frac{\partial \varepsilon_{ij}}{\partial x_k}$ $(x_k = r, \theta, z)$, and factor 2 in the second column of strain matrix arises due to shear strain satisfying $\varepsilon_{ij,k} = \varepsilon_{ji,k}$ $(i \neq j)$. From eq. (5), flexoelectric coefficient μ_{11}, μ_{14}, and μ_{111} corresponds to longitudinal, transverse and shear strain gradient, respectively. In the isotropic material, it meets $\mu_{14} = (\mu_{11} - \mu_{111})/2$.

The inhomogeneous distribution of flexoelectric polarization can generate polarization charges, which, in cylindrical coordinate, are expressed as $\rho_{flexo} = -\left(\frac{1}{r}\frac{\partial (rP_r)}{\partial r} + \frac{\partial P_z}{\partial z}\right)$. According to Eq. (5), we can estimate polarization charges as a form including the second order differential strain components

$$\rho_{flexo} = -\begin{bmatrix} \mu_{11}\left(\frac{\varepsilon_{rr,r}}{r} + \varepsilon_{rr,rr} + \varepsilon_{zz,zz}\right) + 2\mu_{111}\left(\frac{\varepsilon_{rz,z}}{r} + 2\varepsilon_{rz,rz}\right) \\ +\mu_{14}\left(\frac{\varepsilon_{\theta\theta,r} + \varepsilon_{zz,r}}{r} + \varepsilon_{\theta\theta,rr} + \varepsilon_{\theta\theta,zz} + \varepsilon_{zz,rr} + \varepsilon_{rr,zz}\right) \end{bmatrix} \tag{6}$$

Here, $\varepsilon_{ij,kl} = \frac{\partial^2 \varepsilon_{ij}}{\partial x_k \partial x_l}$ is the second-order differential strain, and they meet the commute relationship $\varepsilon_{ij,kl} = \varepsilon_{ij,lk}$. The zero-, first- and second-order differential strain components used here are summarized in Table S1.

In the experiments, the measured tip current is the total current transmitted across the tip–semiconductor contact and is obtained by integrating the local current density over the overall contact area

$$I_{tip} = \iint_{Contact\ area} J\left(V_{ds}, F\right) \cdot dS \tag{7}$$

Therefore, the load dependence of the output current contains two coupled contributions. First, the load-induced flexoelectric polarization modulates the interfacial barrier and thus changes the local current density $J\left(V_{ds}, F\right)$ (polarization effect) at each contact point. Second, the mechanical load enlarges the contact radius and contact area (dimensional effect). This can be

seen from Hertzian contact theory [31], that yields $S_{CA} = \pi a^2 = \pi\left(\frac{3FR}{4E}\right)^{2/3}$, with the contact radius *a*, the Young's modulus E, the tip radius R, and the applied load F. Therefore, the transport modulation in flexoelectronic transistors includes two contributions, i.e., polarization induced barrier modulation that affects the current density (polarization effect), and size expansion that tunes the contact area (dimensional effect).

From Eq. (3), it can be seen that flexoelectric polarization enters the electrostatic equation through the polarization-charge term, $-\nabla\cdot\mathbf{P}$. This term modifies the local electric field and electrostatic potential at the metal–semiconductor interface, thereby changing the band bending and effective interfacial barrier. Because the current density in Eq. (1) depends on both the electric field and carrier concentration, the flexoelectric-polarization-induced electrostatic perturbation further affects the carrier transport. Owing to the strongly nonuniform polarization distribution beneath the nanoscale tip, the resulting barrier modulation is also spatially nonuniform, and is therefore solved numerically by coupling the Poisson, current-density, and continuity equations in COMSOL.

3. Flexoelectric Effect on Centrosymmetric Semiconductor

As a tip is subjected on the semiconductor surface, strain is highly gradient nearby the contact, as sketched in Fig. 1a. As a result, localized lattice distortion is induced to break the inversion symmetry and cause spatially varying ionic displacements. The magnitude and direction of displacements changes nonuniformly, shifting the centers of positive and negative charges and generating local dipole moments. Since these dipoles cannot fully cancel along the strain-gradient direction, a net polarization (or flexoelectric polarization) emerges. The gradient in polarization can further produce ionic charges (or flexoelectric charges) due to departure of net anions and cations [see Fig. 1b]. The flexoelectric charges are negative nearby MS interface and suppress electron accumulation but attract the holes.

To demonstrate the flexoelectric effect, we simulate a 1-μm-thick silicon Schottky diode subjected to a tip-induced load. A tungsten tip (work function: 4.72 eV and radius R = 20 nm) is used to generate gradient strain in the silicon. There are various directions of strain and strain gradient (see Figs. S1 and S2). For illustration, we plot strain ε_r in Fig 1c and $\partial\varepsilon_r/\partial r$ in Fig

1d. The strain is compressive at the contact point and changes to be tensile along the central axis with depth of 7 nm. Such rapid variation in strain causes high strain gradience of 10^7 m^{-1}, and thus enables significant flexoelectric polarization even for silicon (smaller flexoelectric coefficient u_{14} = 0.4 nC/m [32]) [see Fig 1e]. The flexoelectric polarization is vertically downward along the loading direction at the contact central axis, and diffuses in the horizontal direction around axis (see Fig. S3). The maximum polarization is about $P_{Flexo} = 2$ μC/cm² at the contact point and spreads outward with a decreasing intensity. This polarization gradience yields flexoelectric charges that are negative nearby contact and positive in the depth over 5 nm [see Fig 1f].

Because the strain gradient induced by the nanoscale tip is highly non-uniform, the resulting flexoelectric polarization and polarization charges are also distributed non-uniformly beneath the contact. Through the Poisson equation, this spatially varying polarization-charge distribution modifies the internal electrostatic potential and generates a strongly position-dependent electric field. As a result, both the drift and diffusion components of carrier transport become spatially non-uniform, leading to preferential current flow along thickness-direction paths where the local field and band profile are favorable (see Note S2).

As demonstrated above, tip load regulates current transport through two primary mechanisms: the polarization-modulated interface barrier and the conduction area (the tip-silicon contact area). To more clearly illustrate the transport-modulation mechanism, we add a schematic diagram in Fig. 1g. For a spherical indenter of tungsten tip, the applied load could generate flexoelectric polarization and deform the contact geometry (see Fig. 1g-i). As the mechanical load increases, the contact radius and contact area between the spherical tip and semiconductor increase with load (Fig. 1g-ii). This provides an additional geometric contribution to conduction (dimensional effect). Meanwhile, the strain gradient beneath the nanoscale tip becomes stronger to induces more polarization charges. These charges modify the local electrostatic potential and hence the effective interfacial barrier (Fig. 1g-iii).

4. Synergy of Polarization and Dimension Effects on Flexoelectronic Transistors

To reveal the impact of flexoelectric polarization on carrier transport, the current-voltage (I-V) characteristics are explored for Si flexoelectronic transistors using the COMSOL package.

Here, both p- and n-Si are considered for experimental comparisons. The parameters used in the simulation can be found in Table S2. In practical applications, the flexoelectronic transistor operates under finite bias rather than at zero voltage. Therefore, the interfacial transport is governed jointly by the externally applied bias and the mechanically induced flexoelectric polarization. In the present model, both effects are treated self-consistently through the coupled Poisson and carrier-transport equations, so that the local electric field, band profile, and current density are determined by their combined action. Accordingly, the device response should be understood as a joint function of load and voltage, and a suitable operating bias window should be selected to maximize the mechanical modulation efficiency while maintaining stable electrical transport.

p-Si Flexoelectronic Transistors: For a p-Si flexoelectronic transistor, the simulated I–V curves display the expected rectifying behavior of a Schottky contact. With increasing tip load, the forward current increases, whereas the reverse current stays in the off state (Fig. 2a). Figure 2b plots the current as a function of load at V_{ds} = 4.0 V. The current rises rapidly at low loads ($F < 2$ μN) and then approaches saturation near $F \approx 8$ μN. A similar saturation trend has been reported for flexoelectronic transistors in experiments [11]. A similar saturation trend has been reported for flexoelectronic transistors in experiments. Detailed comparison can be found in Note S3. Consistently, the extracted strain sensitivity decreases with load and tends toward zero at high loads (Fig. 2b).

In the simulations (or experiment measurements), the tip current is the total current transmitted across the tip–Si contact, which is obtained by integrating the current density over the contact area. Both the current density and the contact area depend on the tip load. The current density is determined by the interfacial transport barrier tunable by load-induced flexoelectric polarization. Meanwhile, the load could affect the contact radius between tip and Si surface, and thereby adjusts the total current. The output current thus reflects two coupled contributions [see Fig. 2c], i.e., polarization-induced barrier modulation (polarization effect) and contact-area expansion (dimensional effect).

To elucidate the origin of the current saturation, we analyze the load dependence of the current density and the contact size. Owing to the large strain gradients beneath the tip, the

flexoelectric polarization charges are spatially nonuniform, leading to a position-dependent modulation of the interfacial barrier across the contact. As a result, the current density becomes spatially inhomogeneous (Fig. 2d). To quantify this effect, we plot the current-density distribution near the contact region at a small bias of V_{ds} = 0.2 V (Fig. 2e). The current shows little change at small loads (<1 μN), whereas it decreases substantially when the load increases to 6–10 μN. This decrease does not contradict the current increase in Fig. 2b, because the total current depends on both the current density *J* and the contact area *S*. For a spherical indenter, the contact radius is given by [31]

$$a = \left(\frac{3FR}{4E} \right)^{1/3} \tag{8}$$

where *E* is the Young's modulus, *R* is the tip radius, and *F* is the applied load. Consequently, the contact area scales as $S = \pi a^2 \propto F^{2/3}$, as shown in Fig. 2f. At low load, *J* remains nearly constant while *S* increases rapidly, producing a strong current increase dominated by contact-area expansion. With further loading, the reduction in *J* progressively competes with the continued growth of *S*. The balance between these two opposing trends leads to the observed saturation of the total current at large loads.

To connect the load-dependent current density to polarization-induced band modulation, we map the two-dimensional cross-sectional valence-band profile (Fig. 2g). The valence band varies along the radial direction (see Fig. S4 for details), indicating a nonuniform barrier modulation induced by the tip-driven flexoelectric effect. For quantitative analysis, we extract the band profile along the central axis at V_{ds} = 0.2 V (Fig. 2h). Under tip loading, the induced flexoelectric polarization charges distort the local electrostatic potential and, consequently, the band structure. Near the contact interface, negative polarization charges accumulate (Fig. 1f), attracting holes and bending the valence band upward. Away from the interface, positive polarization charges emerge and repel holes (Fig. 2i), leading to downward band bending and forming an energy feature (denoted E_{peak}).

At low load (e.g., F = 1 μN), E_{peak} remains below the interfacial Schottky barrier Φ_0. Hole transport is therefore governed primarily by the unchanged Φ_0 with negligible variation in the current density. As the load increases, the spatial extent of the region with positive polarization

charges expands and strengthens hole repulsion (Fig. 2i), and thus raises E_{peak}. At sufficiently large load (e.g., F = 10 μN), E_{peak} exceeds Φ_0 and becomes the dominant transport barrier, which continues to increase with load. Consequently, the interfacial current density decreases markedly at high loads. Note that, the reduction in E_{peak} would be limited by the accumulated holes at a large load (see Fig. S5). As a result, holes experience an increasingly limited barrier lowering under larger loads, which directly causes the reduction in local current density observed in Fig. 2e.

n-Si Flexoelectronic Transistors: For the n-Si flexoelectronic transistor, the simulated output also exhibits rectifying I–V behavior (Fig. 3a). In the on state (V_{ds} = −1 V), the current depends only weakly on the applied tip load (Fig. 3a and inset), in sharp contrast to the p-Si case. A closer examination reveals a non-monotonic load dependence (Fig. 3b). The current increases rapidly at small forces, then rises more gradually and reaches a maximum at a critical load of ~18 μN, after which it decreases with further loading. The extracted strain sensitivity declines with increasing load (Fig. 3c), with a peak value of ~200.

This non-monotonic response has also been observed in flexoelectronic transistor [11], and their similarity has been demonstrated in Note S3. We attribute this behavior to the competition between contact-area expansion (dimensional effect) and flexoelectric-charge-induced barrier modulation (polarization effect). To understand the competition, we first isolate the polarization contribution by extracting the zero-bias conduction-band profile along the central axis (Fig. 3d). Tip loading generates negative flexoelectric polarization charges near the interface (Fig. 1f), which repel electrons and bend the conduction band upward (inset of Fig. 3d). This increases the effective interfacial barrier and reducing the interfacial current density (Fig. 3e). With increasing load, the negatively charged region expands, strengthening electron depletion and further enhancing the barrier (see Fig. S6). Meanwhile, the mechanical load enlarges the tip–Si contact area (Fig. 3f). The total current therefore reflects the balance between a decreasing current density and an increasing conducting area.

At low loads, polarization is relatively weak. Hence, the reduction in current density is modest and the current increase is dominated by contact-area growth. At higher loads, barrier enhancement becomes sufficiently strong to suppress the current density more rapidly,

eventually overcoming the geometric gain from area expansion. This crossover produces the observed current maximum followed by a load-induced decay.

To further clarify the respective roles of these two mechanisms, we decouple the polarization effect and the dimensional effect in separate simulations by either fixing the contact area or removing the flexoelectric polarization. The resulting current–load characteristics and their comparison with the fully coupled case are presented in Note S4, which quantitatively demonstrates the individual contributions of area change and flexoelectricity to the transport response.

5. Dimension-Polarization Effect on Flexoelectronic Transistors

Considering the size-dependent nature of the flexoelectric effect [27], we further examine how the tip radius influences device performance. To this end, the I–V characteristics and the load-dependent current are evaluated for both p- and n-type silicon using tips of varying radii.

For a fixed load (F = 6 μN), the output current of both p-type (Fig. 4a) and n-type (Fig. 4c) flexoelectric transistors increases markedly with increasing tip radius. In p-type devices, the current exhibits a characteristic saturation trend as the applied load increases. Notably, the magnitude of current variation becomes progressively larger for devices with larger tip radii, reflecting an enhancement of strain sensitivity (Fig. 4b). This phenomenon arises because a larger tip radius reduces the strain gradient and thus diminishes the flexoelectric polarization charge (Fig. 4e), weakening the polarization effect. However, the increase in radius substantially amplifies the contact-area growth with load, as evidenced by the steeper slope in Fig. 4f. As a result, prior to the onset of current saturation, the dimensional (contact-area) contribution dominates over the polarization-induced suppression, yielding an enhanced flexoelectric response.

A similar trend is observed in n-type transistors. For all tip radii examined, the current increases, and reaches a maximum value, and finally decreases with load. However, the critical load with a maximum current expands with increasing tip radius, and the overall variation becomes more pronounced (Fig. 4d). This behavior is again attributable to the interplay between two competing mechanisms. A larger tip radius attenuates the polarization effect while strengthening the dimensional effect. Consequently, the dimension-driven increase in current

is amplified, whereas the polarization-driven reduction is mitigated, resulting in a more prominent load-dependent response.

The size effect discussed here mainly refers to the dependence of device response on the tip radius, as shown in Fig. 4. Because flexoelectric polarization originates from strain gradients, reducing the characteristic tip size enhances the strain gradient [see Note S5] and strengthens the polarization-induced barrier modulation. At the same time, increasing the tip size enlarges the contact radius and amplifies the dimensional contribution to transport. Therefore, the geometry size in flexoelectronic transistors should be regarded as a tunable design parameter that balances polarization and dimensional effects, rather than as a simple limiting factor. The optimal size depends on whether the target is stronger barrier modulation, higher current sensitivity, or better mechanical robustness.

6. **Conclusion**

In conclusion, this work establishes a unified theoretical picture for charge transport in silicon-based flexoelectronic transistors under nanoscale tip loading. It shows that the load regulates the current through two intrinsically coupled mechanisms: strain-gradient-induced flexoelectric polarization that modulates the interfacial transport barrier and load-driven contact-size expansion that contributes an additional dimensional gain to conduction. Their opposite impacts on p- and n-type devices lead to a characteristic polarization–dimension competition. In addition, we further demonstrate that tip-radius engineering provides a practical knob to rebalance these competing effects. Larger radii weaken the polarization contribution while amplifying the dimensional contribution, thereby improving the load-dependent response and enhancing strain sensitivity. This study not only gives an insight into the nanoscale flexoelectronic physics, but also offers a design guidance for optimizing flexoelectronic sensors based on centrosymmetric semiconductors.

Acknowledgements

This work was supported by the National Natural Science Foundation of China (Grant No. 62404125), the Natural Science Foundation of Hubei Province (Grant No. 2024AFB359), the Youth Talent Project of the Science and Technology Research Program of the Education Department of Hubei Province (Grant No. Q20241213), the Guangdong Basic and Applied Basic Research Foundation (Grant No. 2025A1515011971), and the Basic Research Programs of Taicang, 2024 (Grant No. TC2024JC40).

Author Declarations: The authors have no conflicts to disclose.

Reference

[1] W. Wu *et al.*, Nature **514**, 470 (2014).

[2] W. Wu and Z. L. Wang, Nature Reviews Materials **1**, 16031 (2016).

[3] Q. Yu, R. Ge, J. Wen, T. Du, J. Zhai, S. Liu, L. Wang, and Y. Qin, Nature communications **13**, 778 (2022).

[4] Q. Yu, R. Ge, J. Wen, Q. Xu, Z. Lu, S. Liu, and Y. Qin, Nature communications **15**, 4245 (2024).

[5] W. Gao, S. Liu, and Y. Qin, Research **9**, 1048 (2026).

[6] J. W. Stewart, J. H. Vella, W. Li, S. Fan, and M. H. Mikkelsen, Nat Mater **19**, 158 (2020).

[7] U. Schroeder, M. H. Park, T. Mikolajick, and C. S. Hwang, Nature Reviews Materials **7**, 653 (2022).

[8] F. Li, B. Wang, X. Gao, D. Damjanovic, L.-Q. Chen, and S. Zhang, Science **389**, eadn4926 (2025).

[9] R. Guo *et al.*, Nature communications **11**, 2571 (2020).

[10] S. M. Park *et al.*, Nature communications **11**, 2586 (2020).

[11] L. Wang, S. Liu, X. Feng, C. Zhang, L. Zhu, J. Zhai, Y. Qin, and Z. L. Wang, Nature nanotechnology **15**, 661 (2020).

[12] D. Guo *et al.*, Science advances **9**, eadd3310 (2023).

[13] X. Jia, R. Guo, J. Chen, and X. Yan, Advanced Functional Materials **35**, 2412887 (2025).

[14] T. D. Nguyen, S. Mao, Y. W. Yeh, P. K. Purohit, and M. C. McAlpine, Adv. Mater. **25**, 946 (2013).

[15] P. Zubko, G. Catalan, and A. K. Tagantsev, Annual Review of Materials Research **43**, 387 (2013).

[16] C. A. Mizzi, A. Y. Lin, and L. D. Marks, Phys. Rev. Lett. **123**, 116103 (2019).

[17] C. A. Mizzi and L. D. Marks, Nano Lett. **22**, 3939 (2022).

[18] F. Zhang *et al.*, Phys. Rev. Lett. **122** (2019).

[19] S. Das, B. Wang, T. R. Paudel, S. M. Park, E. Y. Tsymbal, L.-Q. Chen, D. Lee, and T. W. Noh, Nature communications **10**, 537 (2019).

[20] K. D. Breneman, W. E. Brownell, and R. D. Rabbitt, PLoS One **4**, e5201 (2009).

[21] F. Vasquez-Sancho, A. Abdollahi, D. Damjanovic, and G. Catalan, Adv. Mater. **30**, 1705316 (2018).

[22] M. Wu *et al.*, Nano Lett. **21**, 2946 (2021).

[23] M.-M. Yang, D. J. Kim, and M. Alexe, Science **360**, 904 (2018).

[24] W. Huang, X. Yan, S. R. Kwon, S. Zhang, F.-G. Yuan, and X. Jiang, Applied Physics Letters **101** (2012).

[25] S. M. Park, B. Wang, L.-Q. Chen, T. W. Noh, S. M. Yang, and D. Lee, Applied Physics Reviews **8** (2021).

[26] Y. Zhang, J. Chen, R. Yu, S. Liu, and Y. Qin, ACS nano **19**, 6705 (2025).

[27] M. Majdoub, P. Sharma, and T. Cagin, Physical Review B—Condensed Matter and Materials Physics **77**, 125424 (2008).

[28] S. M. Sze, Y. Li, and K. K. Ng, *Physics of semiconductor devices* (John wiley & sons, 2021).

[29] G. Hu, Y. Zhang, Y. Chao, F. Huang, M. Li, M. Liu, and W. Huang, Nano Energy, 111440 (2025).

[30] F. Huang, Y. Chao, Q. Yang, M. Dan, Q. Chen, G. Hu, and W. Huang, Nano Energy **134**, 110535 (2025).

[31] A. C. Fischer-Cripps, *Introduction to contact mechanics* (Springer, 2000).

[32] J. Hong and D. Vanderbilt, Physical Review B—Condensed Matter and Materials Physics **88**, 174107 (2013).

Figures and captions

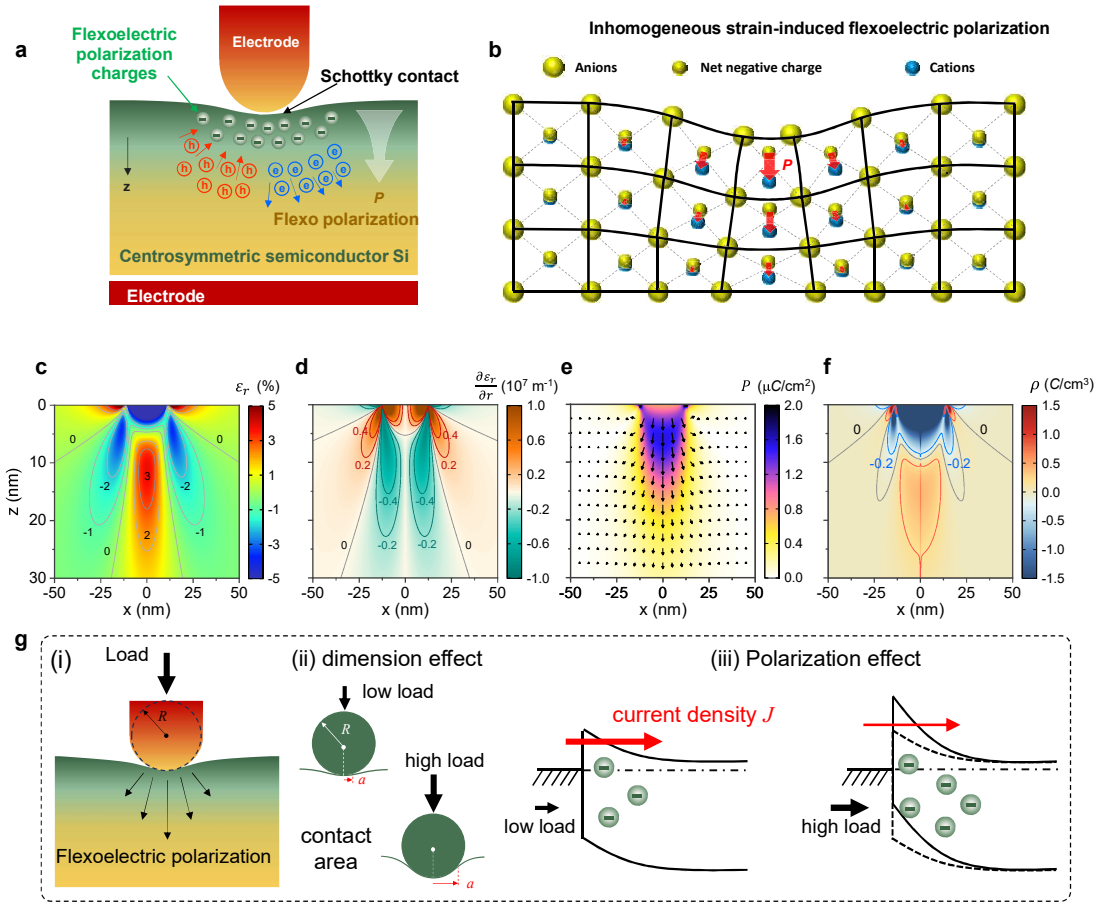

Fig 1. The flexoelectric effect caused by strain gradient in Si. (a) The device structure and modulation mechanism of carrier transport by the flexoelectric effect. (b) The origination of strain gradient-induced flexoelectric polarization. The calculated distribution of strain (c), strain gradient (d), flexoelectric polarization and direction (e), and polarization charges (f). Here, the tip radius and applied force are 20 nm and 10 μN, respectively. (g) Schematic of tip-load-induced flexoelectric polarization (g-i), Contact conditions (g-ii) and band structures (g-iii) of the tip-silicon interface under low and high load. Here, R is the radius of the spherical indenter tip, a is the contact radius between the tip and silicon.

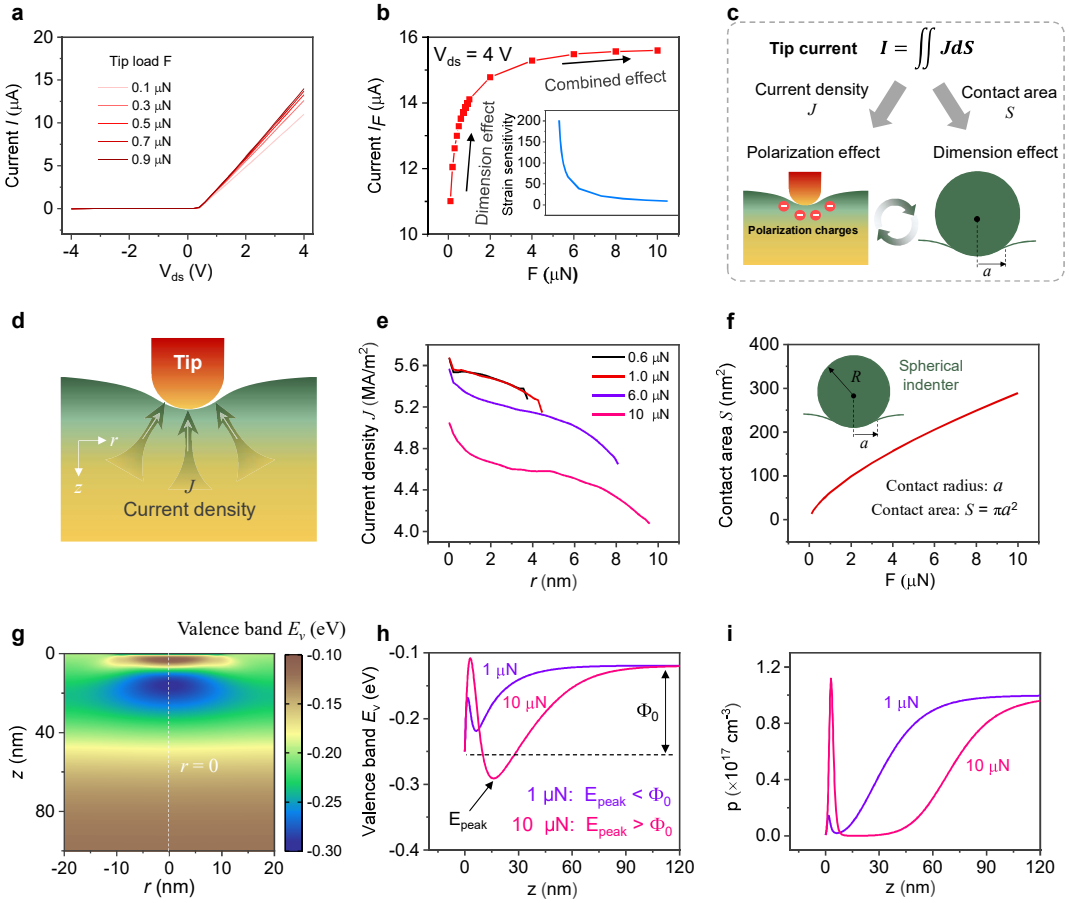

Fig 2. The modulation mechanism in p-Si flexoelectronic transistors. (a) The I-V characteristics under load. The inset demonstrates the predominated modulation mechanism of flexoelectric charges. (b) The load-dependent current and strain sensitivity (inset) at bias voltage $V_{ds} = 4.0$ V. (c) Tip current is modulated through two primary mechanisms: changes in current density J driven by flexoelectric polarization, and variations in contact area S induced by dimension effects. (d) The schematic of current density distribution at the silicon-tip contact interface. (e) The current density distribution at $V_{ds} = 0.2$ V. (f) The contact area S varying with load. Here, the spherical indenter tip has a radius of R, establishing a contact radius of a and a contact area of S with the silicon substrate. (g) Two-dimensional cross-sectional valence band distribution map of silicon crystal at $V_{ds} = 0.2$ V for F = 10 μN. (h) The energy band diagram along the central axis at $V_{ds} = 0.2$ V for F = 1 and 10 μN. Here, the initial interfacial barrier is Φ_0, and the peak of the downward band bending induced by positive flexoelectric charges is E_{peak}. (i) The hole concentration along the central axis at $V_{ds} = 0.2$ V for F = 1 and 10 μN.

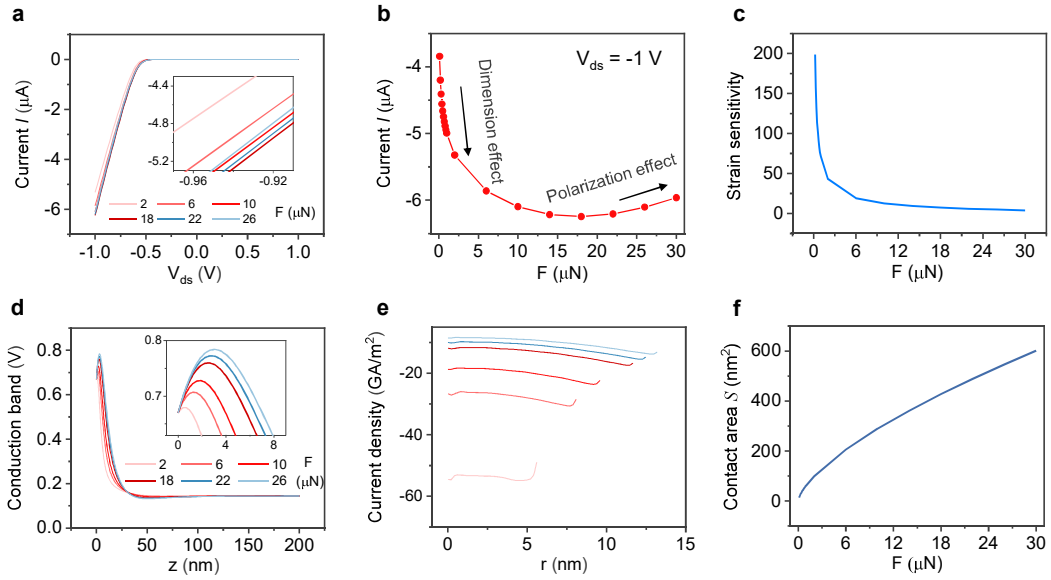

Fig 3. The modulation mechanism in n-Si flexoelectronic transistors. (a) The I-V characteristics under load, and partial enlarged view (inset). (b) The reverse current ($V_{ds} = -1.0$ V) as a function of load. (c) The strain sensitivity at $V_{ds} = -1.0$ V. (d) The zero-bias conduction band diagram along the central axis, and partial enlarged view (inset). (e) The current density distribution at $V_{ds} = -1.0$ V. (f) The contact area S varying with load.

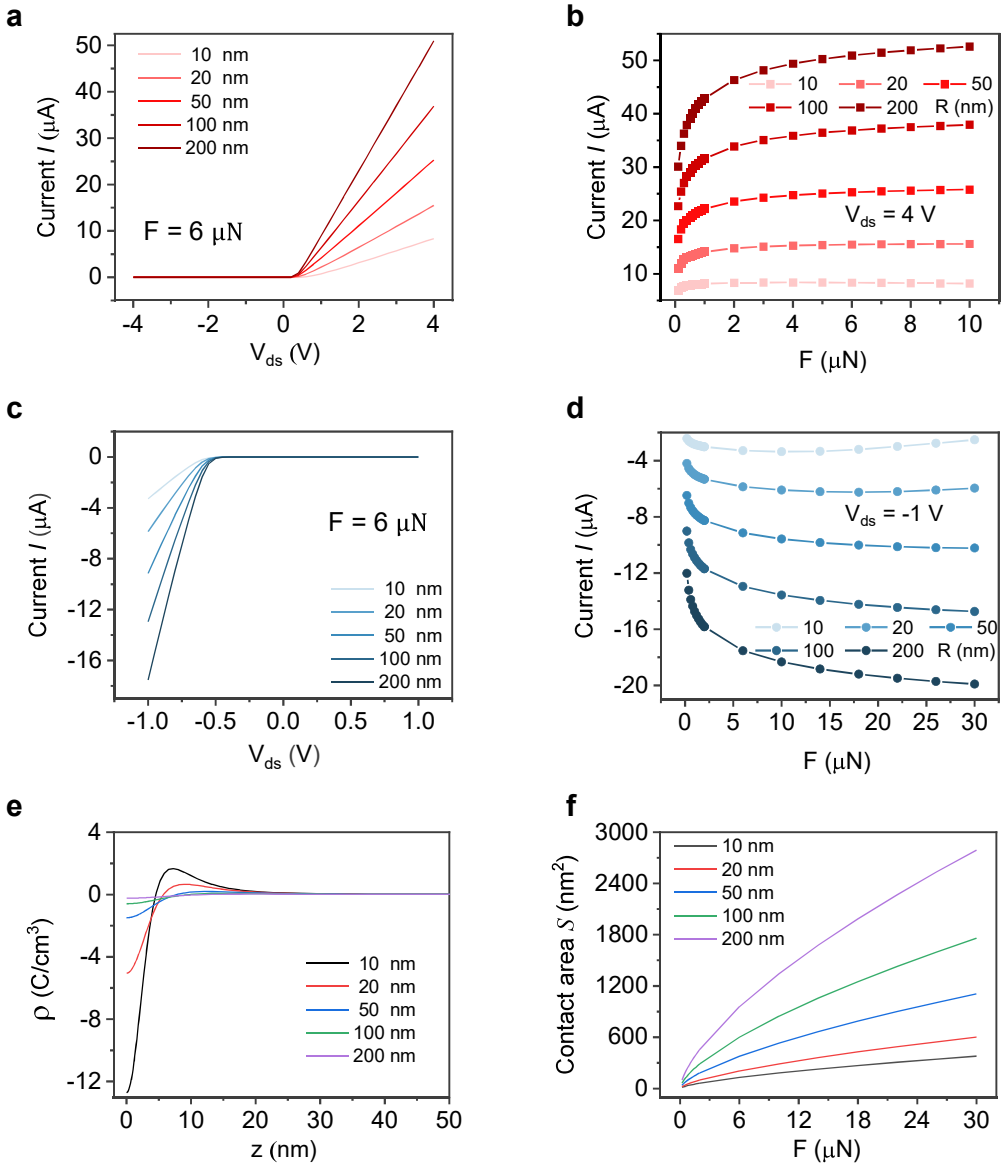

Fig 4. The tip dimensions modulation mechanism in flexoelectric transistors. (a) The I-V characteristics of p-Si under F = 6 μN with varied tip radius. (b) The current as a function of load for p-Si under varied tip radius at $V_{ds} = 4.0$ V.(c) The I-V characteristics of n-Si under F = 6 μN with varied tip radius. (d) The current as a function of load for n-Si under varied tip radius at $V_{ds} = -1.0$ V. (e) The distribution of flexoelectric charge along the central axis for tips of different radius. (f) The variation of contact area *S* with load for tips of different radius.